Mass Composition and Cross-section from the Shape of Cosmic Ray Shower Longitudinal Profiles

S. Andringa, R. Conceição, M. Pimenta

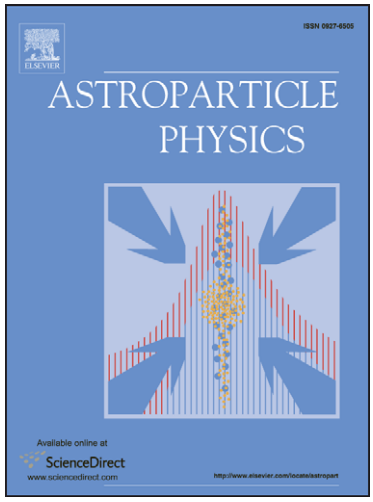

Mass Composition and Cross-section from the Shape of Cosmic Ray Shower Longitudinal Profiles

S. Andringa, R. Conceição, M. Pimenta

PII: S0927-6505(10)00183-0
DOI: 10.1016/j.astropartphys.2010.10.002
Reference: ASTPHY 1527

To appear in: *Astroparticle Physics*

Received Date: 12 April 2010
Revised Date: 27 September 2010
Accepted Date: 3 October 2010

Please cite this article as: S. Andringa, R. Conceição, M. Pimenta, Mass Composition and Cross-section from the Shape of Cosmic Ray Shower Longitudinal Profiles, *Astroparticle Physics* (2010), doi: 10.1016/j.astropartphys.2010.10.002

Mass Composition and Cross-section from the Shape of Cosmic Ray Shower Longitudinal Profiles

S. Andringa[a]*, R. Conceição[a] and M. Pimenta[a,b]

a) LIP, Av. Elias Garcia, 14-1. 1000-149 Lisboa, Portugal

b) Dep. Física, IST, Av. Rovisco Pais, 1049-001 Lisboa, Portugal

Abstract

The longitudinal development of extreme energy cosmic ray showers has a characteristic "Universal Shower Profile" when normalized and translated to the shower maximum. Experimentally accessible observables can be defined to parametrize the average shape and characterize each event. By describing the full shape of the profile, information related to the first hadronic interactions and primary particle type can be extracted. A shape variable which measures the distance from the first interaction to the depth of maximum can lead to a cosmic ray composition analysis with independent extraction of the primary cross-sections.

Keywords: high energy cosmic rays; extensive air showers; logitudinal profiles; primary mass composition; cross-section; hadronic models

1 Introduction

Very high energy cosmic rays can not be directly detected but their interactions in the atmosphere produce extensive air showers with a high number of lower energy particles. Only few of these particles can be detected at the ground but the development of the shower can also be observed indirectly through the fluorescence light emitted by the air nitrogen molecules, proportional to the varying number of low energy shower electrons that excite

*Corresponding author: Sofia Andringa (sofia@lip.pt), LIP, Av. Elias Garcia, 14-1. 1000-149 Lisboa, Portugal, Tel:+351 21 797 38 80, Fax:+351 21 793 46 31.

them at a given stage. The first high energy interactions at the start-up of the shower can not be observed directly with this technique as there are not enough particles to produce detectable light.

The maximum number of particles is related to the primary particle energy and is the main characteristic of the shower together with the depth at which the maximum is reached. The mean depth of shower maximum at a given energy can be used to infer statistically the cosmic ray composition, in terms of primary particle types [1]. Shower initiated by heavy nuclei, having a higher cross-section and multiplicity, will reach the maximum faster in average and with less event-to-event fluctuations than those expected for proton initiated showers.

We propose that more information can be extracted from the full shape of the shower longitudinal profiles and try to identify the parameters that can be connected with experimentally accessible observables. In this way, it will be possible to extract more information in an event-by-event basis and to separate the analyses of primary cosmic ray composition and first interaction cross-sections. We have tested the parametrization in simulated samples of proton and iron primaries, with energies between $10^{17.5}$ eV and 10^{20} eV, using different hadronic models (QGSJet-II.03 [2] and EPOS 1.99 [3]) in showers developed using CONEX [4].

2 Shower Profile Shape Variables

The longitudinal profile of extensive air showers is mostly determined by the maximum number of particles reached (N_{max}) and the corresponding depth (X_{max}) and have a characteristic "universal" shape after translation to $X' = X - X_{max}$ and normalization $N' = N/N_{max}$ [5]. In figure 1, these transformations are exemplified for simulated samples of different primaries and energies.

Different parametrization of the shower profiles have been proposed in the literature. Studies have shown that two extra parameters are needed for the full description of the general profiles, but there can be strong correlations between them [6, 7]. A widely use, successful parametrization is the Gaisser-Hillas profile [8], which can be written in terms of the new variables, X', N', as follows:

$$N' = \left(1 - \frac{X'}{X'_0}\right)^{-\frac{X'_0}{\lambda}} \exp\left(-\frac{X'}{\lambda}\right) \tag{1}$$

where two extra parameters appear: λ identified with an effective interaction length and $X'_0 = X_0 - X_{max}$ being X_0 related with the point of first

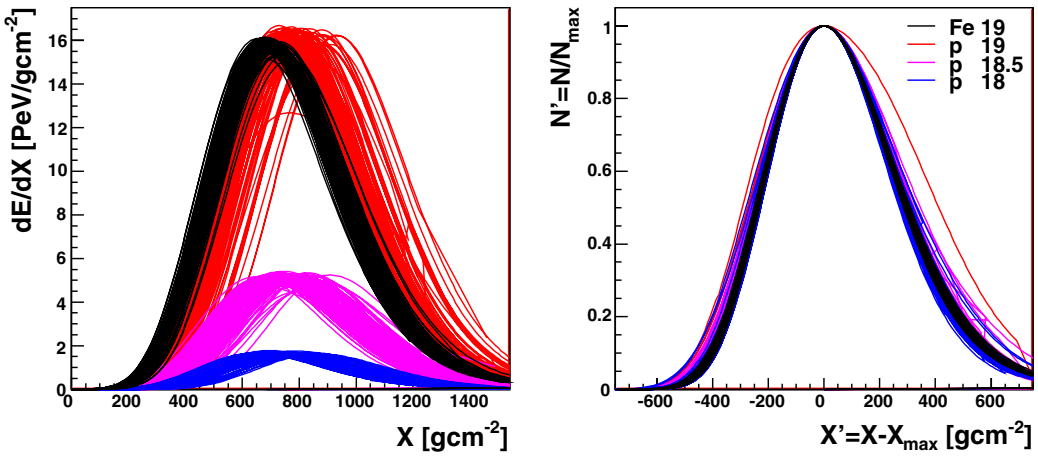

Figure 1: Longitudinal profiles for 100 showers of different energies and primary particles, shown as $dE/dX(X)$, proportional to $N(X)$, (left plot) and $N'(X')$ (right plot).

interaction. However, not only the physical meaning of the parameters is not exact but they are also difficult to relate to the "universality" features seen in fig. 1. We investigate the relation between parameters that separate the more universal features from the details of each shower.

The Gaisser-Hillas profile (equation 1) can be written as:

$$N' = \exp\left(-\frac{X'_0}{\lambda}\log\left(1-\frac{X'}{X'_0}\right)-\frac{X'}{\lambda}\right)$$
$$= \exp\left(-\frac{X'^2}{2|X'_0\lambda|}\right)\prod_{n=3}^{\infty}\exp\left(\frac{1}{n}\frac{X'_0}{\lambda}\left(\frac{X'}{X'_0}\right)^n\right) \quad (2)$$

$$N' = \exp\left(-\frac{1}{2}\left(\frac{X'}{L}\right)^2\right)\prod_{n=3}^{\infty}\exp\left(-\frac{R^{n-2}}{n}\left(-\frac{X'}{L}\right)^n\right) \quad (3)$$

where, from a Taylor expansion of the logarithm around the maximum ($X' = 0$), the profile shape becomes more evident. The first term in X' cancels, leaving a gaussian with a characteristic width L=$\sqrt{|X'_0\lambda|}$, and distortions governed by a shape parameter R=$\sqrt{\lambda/|X'_0|}$. While for positive X', the even and odd terms in R have partial cancellation, all terms contribute to the distortion in the region of negative X'. Figure 2 shows how the shape changes for different values of both parameters.

To compare the new parameters L and R with the old λ and X'_0, we fit different realizations of an ideal profile assuming statistical deviations for an

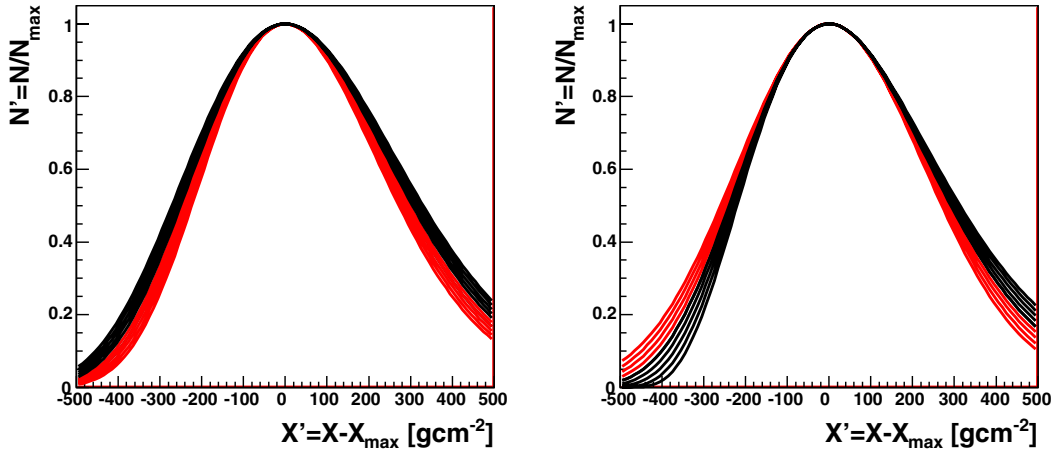

Figure 2: Different profiles obtained by varying L (left plot) and R (right plot) around central values of L=225 g cm^{-2} (with 5 g cm^{-2} steps) and R=0.25 (with 0.05 steps).

observation of 200 photons at maximum and X bins of 30 g cm^{-2}. The result in fig 3 shows that both λ and X_0' can be (mis)reconstructed with up to 100% variations, and are strongly correlated, while L and R are more independent and stable variables, as expected. In particular L varies only by less than 10%.

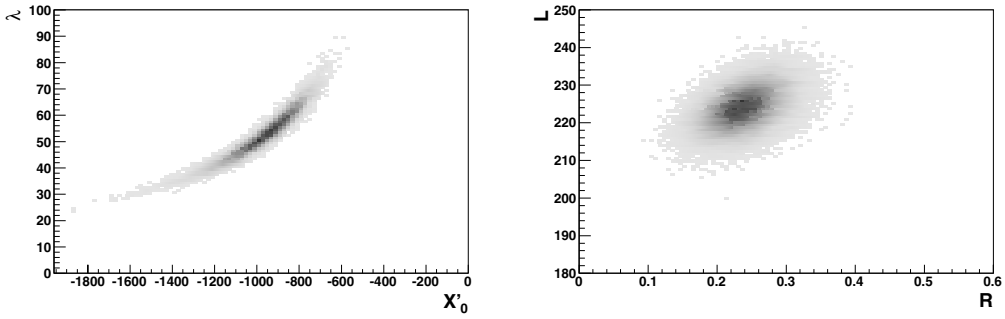

Figure 3: Correlation between λ and X_0' (left) and L and R (right) obtained for the fit of different realizations of the same ideal profile, with $N_{max} = 200$ and X bins of 30 g cm^{-2}.

We thus prefer to eq. 1 in terms of L and R (noticing X_0' is always

negative) as:

$$N' = \left(1 + \frac{RX'}{L}\right)^{R^{-2}} \exp\left(-\frac{X'}{LR}\right) \tag{4}$$

The shower visible energy (E_{em}), mainly deposited by the low energy electrons, is proportional to the total number of particles and thus to the profile integral. Corrections due to the invisible energy carried away by muons and neutrinos vary according to the primary particle type, energy, and hadronic model considered, but are expected to be around 5% to 10%, and to decrease as energy increases [9]. The fraction of energy deposited at shower maximum, $\frac{dE}{dX}\Big|_{max}$ proportional to N_{max}, has event-by-event variations of the same size, which are naturally reflected in fluctuations of the new parameters. The full integral of the profile, can be written in terms of the usual Gamma function, as:

$$\int N'(X')dX' = E_{em}/\frac{dE}{dX}\Big|_{max} = (LR)A^{-A}\exp(A)\Gamma(A+1) \tag{5}$$

$$\int N'(X')dX' = E_{em}/\frac{dE}{dX}\Big|_{max} \sim (LR)\sqrt{2\pi A} = \sqrt{2\pi}L. \tag{6}$$

where $A = R^{-2}$ and the approximation by $\sqrt{2\pi}L$ results in an small underestimation of the integral (by <1% for R<0.35 and ∼9% for the extreme value of R=1).

The average shower profile expressed in X' and N' for each sample provides meaningful information that can be extracted in the parameters L and R in equation 4. The results of fits for the different sets of simulated events and fitting conditions are shown in Table 1. Considering only the QGSJet-II samples at 10^{19}eV, the variation of the parameter L is less than 2%, while the parameter R distinguishes the proton and iron samples at a level around 15%. The information about the first hadronic interactions is dilluted after the electromagnetic shower maximum is reached, so the parameters are better determined when the pre-maximum shower profile is seen [1]. We conclude that by fixing the L parameter, we can isolate in R most of the information, maximizing the sensitivity to the primary particle type, consistently for all the studied samples, and increasing the separation to a 30% level for the QGSJet-II samples at 10^{19}eV.

[1]Not only the later part of the profile $X' > 0$ has less information on R, but also in this region the fluorescence light is contaminated by light scattered from the accumulated Cherenkov beam created by the shower particles. While the direct Cherenkov light can be avoided by geometrical selection of the events, large amounts of Cherenkov light present after X_{max} have to be statistically accounted for in the data reconstruction [10].

Sample	L_{USP}	R_{USP}	R_{Lmed}	$R_{negX'}$	L dist.	R dist.
Q Fe 20.0	231.4	0.238	0.246	0.266	232.8 (2.7)	0.269 (0.022)
Q Fe 19.5	228.9	0.249	0.254	0.270	230.4 (2.9)	0.272 (0.024)
Q Fe 19.0	226.4	0.260	0.263	0.276	228.4 (3.3)	0.277 (0.027)
Q Fe 18.5	224.3	0.271	0.274	0.283	226.6 (3.6)	0.285 (0.030)
Q Fe 18.0	222.7	0.284	0.284	0.291	225.1 (4.1)	0.293 (0.033)
Q Fe 17.5	220.9	0.294	0.293	0.298	223.7 (4.6)	0.301 (0.038)
Q P 20.0	239.4	0.217	0.209	0.180	240.6 (8.8)	0.178 (0.076)
Q P 19.5	234.5	0.220	0.217	0.193	235.8 (7.4)	0.192 (0.070)
Q P 19.0	230.3	0.226	0.224	0.208	231.6 (6.5)	0.207 (0.066)
Q P 18.5	226.7	0.235	0.234	0.224	228.2 (6.9)	0.223 (0.069)
Q P 18.0	223.2	0.245	0.244	0.241	225.1 (7.6)	0.240 (0.073)
Q P 17.5	219.7	0.255	0.255	0.260	222.1 (8.9)	0.257 (0.081)
E P 19.0	232.9	0.212	0.209	0.185	234.2 (8.0)	0.169 (0.084)
E Fe 19.0	227.1	0.249	0.256	0.270	229.1 (3.1)	0.260 (0.023)

Table 1: L (in g cm^{-2}) and R obtained for different samples, labeled Q for QGSJet-II and E for EPOS 1.99, and according to primary particle (Fe/P) and log(E/eV). The first columns show the results of the fits to the average USP constructed from the 20000 events: first, for $X' \in$[-500,500] g cm^{-2}, with both parameters free; next, the parameter L is fixed - with the average value obtained for proton and iron showers at each energy (and model); and then the fit is performed for $X' \in$[-400,100] g cm^{-2}. The last two columns show the mean (rms) values of L$= E_{em}/\frac{dE}{dX}\Big|_{max}/\sqrt{2\pi}$, and R obtained from the fit to individual profiles (in the same conditions as in the last USP fit).

The parameter L is thus a characteristic shower length with a slow logarithmic energy evolution, small dependence on the particle type and event-by-event fluctuations of the order of a few percent. The energy evolution can be taken into account, but - at a fixed energy - the value of L can be considered constant for the following analyses (we will use the average between the proton and iron values). The parameter R, on the contrary, has small impact on the total integral and energy, but represents an asymmetry which is sensitive to primary particle types [7]. It can be used to characterize each individual event[2].

[2]In data analysis, one can identify each shower energy (by N_{max} alone, or by the standard methods) and determine an average $\bar{L}$ from the USP fit for each energy sample.$\bar{L}$ can be used as an input in fits to individual showers if needed, while R will not alter the energy determination. R can be obtained for each event in the subset of showers for which a longer part of the profile is seen.

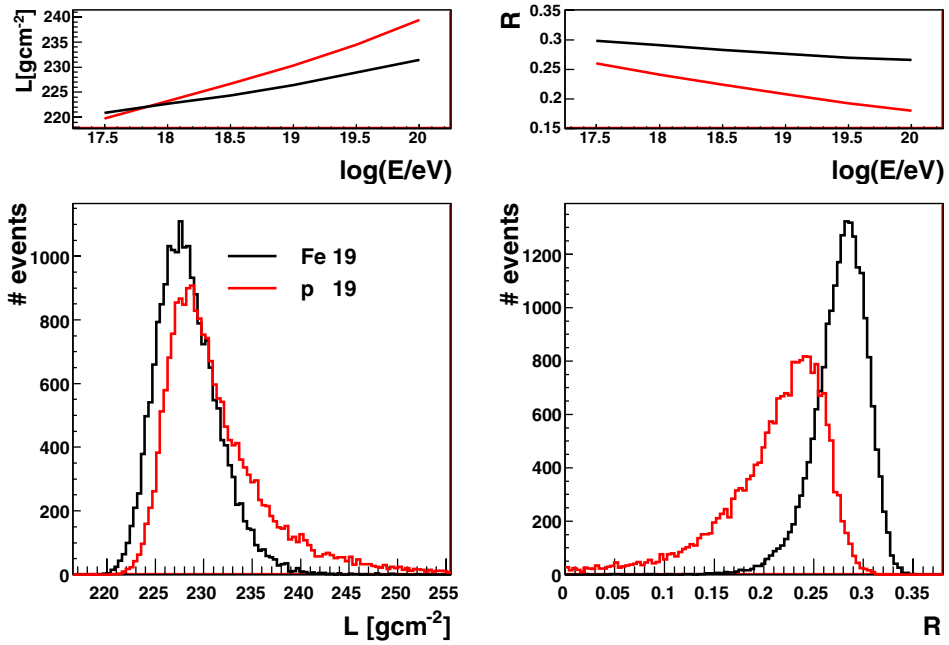

Figure 4: Distributions of L (left plot) and R (right plot), for proton and iron primaries at fixed energy $log(E/eV) = 19$. The energy evolution of the mean values of the parameters is shown in the top plots, for proton (red) and iron (black) showers.

Figure 4 shows the distribution of the event-by-event values of L, obtained from the energy as in equation 6, and R, obtained from the fit of the profile to the region $X' \in [-400, 100]$ g cm^{-2} with a fixed L, in simulated samples of proton and iron primaries at $\log E/eV = 19$. The mean and rms of the distributions can also be seen in table 1 for the other samples. The separation between proton and iron increases with energy in the studied range, while there is a crossing in L for $\log(E/eV) < 18$, the distinction in R is improved.

Hence, R is a new variable for cosmic ray composition analyses. Notice that not only the mean value of R is sensitive to composition, but also its fluctuations are larger for proton than for iron initiated showers, as expected.

3 Accessing the First Interactions on an Event-by-event Basis

The parameter R is obtained uniquely from the shape of the normalized profile translated to the maximum, and is experimentally independent from X_{max}. It measures the growing rate of the number of particles from the first interaction to the depth at which the maximum is reached, and is determined independently of the translations induced by the depth of the first interaction on X_{max}.

The relation between R and X_{max} is shown in fig. 5(top), for samples of proton and iron showers generated according to two different models. While typical values of R are different for iron and proton, proton showers also exhibit larger fluctuations in shape and R values. Naturally, R is correlated with X_{max}, as larger X_{max} imply either a very deep first interaction (X_1) or a slow degradation of the energy until the maximum is reached. However, as an independent variable, R can reinforce the proton/iron separation of the showers obtained from X_{max} alone. By combining the two variables, not only the analysis of composition can be improved, but the different contributions to X_{max} can also be separated.

In figure 5(center), R is related to $\Delta = X_{max} - X_1$, that is obtained from the generator information. The correlation of R with Δ is larger than with X_{max}, since the smearing caused by X_1 is removed. The values of R defined above, do not only help in the composition information but, by keeping record of the individual shower shape, measure the distance to the first interaction point.

The showers can be separated according to $\Delta = X_{max} - X_1$, as done in tab. 2 and fig. 6(left), which show the corresponding USPs and the L and R values. Although the distance in depth Δ is reflected also in the parameter L (at a few % level), the parameter R has a much larger sensitivity. From the table, it can be seen that as Δ increases, R decreases in an approximately linear way, but also the dispersion in R increases. Negative values of R, unexpected by construction, can arise and are an indication of a particular class of events, where the evolution towards shower maximum does not follow the usual Gaisser-Hillas profile (examples can be seen in fig. 6(right)).

In any case, Δ gives a more precise physical meaning to the shape of the shower. It is independent of the cross-section of the primary interaction, but depends on a convolution of the hadronic interactions parameters, as the multiplicity, inelasticity or the lower energy cross-sections. A calibration of Δ(R) can be done (as shown in fig. 5(center)), leading to an estimate of $X_1 = X_{max} - \Delta$ in an event-by-event way. Finally, distributions of Δ

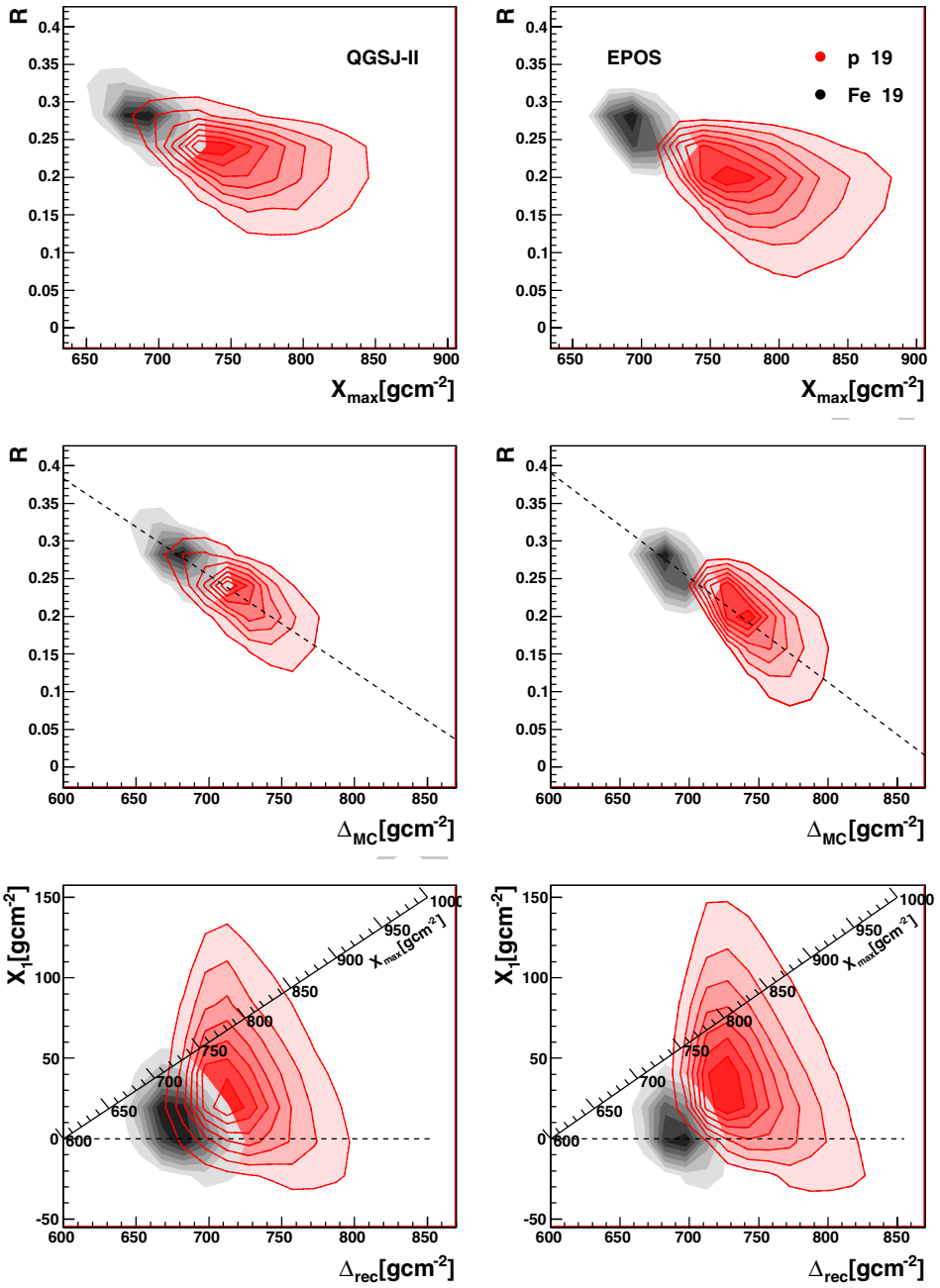

Figure 5: In the top plots, the reconstructed R and X_{max} obtained for simulated samples of proton and iron showers at energy $\log(E/eV) = 19$ with two different hadronic models, QGSJet-II (left) and EPOS (right), are shown. In the middle plots, R is compared with $\Delta = X_{max} - X_1$ (taken from the simulation), for the same samples; the dashed line shows the average calibration obtained from table 2. In the bottom, Δ and X_1 are reconstructed from R and X_{max} (the $X_{max} = \Delta + X_1$ axis is shown for convenience).

Sample	L_{USP}	R_{USP}	R_{Lmed}	$R_{negX'}$	L dist.	R dist.
Fe 19.0	226.4	0.260	0.263	0.276	228.4 (3.3)	0.277 (0.027)
Δ 665.5 (6.5)	224.9	0.264	0.270	0.291	226.7 (2.5)	0.295 (0.016)
Δ 686.1 (6.9)	226.9	0.260	0.263	0.272	228.8 (2.9)	0.273 (0.020)
Δ 709.2 (6.8)	228.9	0.255	0.255	0.251	230.6 (3.4)	0.252 (0.028)
Δ 733.5 (6.4)	230.9	0.250	0.246	0.230	232.4 (4.0)	0.229 (0.034)
P 19.0	230.3	0.226	0.224	0.208	231.6 (6.5)	0.207 (0.066)
Δ 690.2 (6.9)	226.5	0.244	0.248	0.256	227.9 (2.8)	0.258 (0.019)
Δ 713.4 (7.1)	228.2	0.234	0.235	0.234	229.5 (3.7)	0.253 (0.025)
Δ 736.4 (7.1)	230.6	0.225	0.219	0.205	231.8 (4.9)	0.204 (0.036)
Δ 760.9 (7.1)	233.2	0.217	0.202	0.173	234.3 (6.8)	0.172 (0.054)
Δ 785.7 (7.1)	235.6	0.210	0.191	0.143	236.5 (8.4)	0.142 (0.078)

Table 2: L (in g cm^{-2}) and R obtained for iron (top) and proton (bottom) showers, divided by 25 g cm^{-2} in Δ (mean and rms are shown), from USP fits in the same conditions as table 1. The mean and rms of L and R distributions of individual showers are shown in the last columns.

and X_1 reconstructed from R and X_{max} are shown in fig. 5(bottom); the corresponding X_{max} axis is also shown, but by isolating the two contributions we get a more physical way to look at the proton/iron separation, and to try to investigate the different ingredients of the hadronic models.

The one-dimensional distributions of $X_1 = X_{max} + \Delta(\mathrm{R})$ reconstructed for proton and iron showers are shown in fig. 7. The distributions are fitted to an exponential in $\overline{X_1}$ convoluted with a gaussian. The obtained values for the exponential parameter are in reasonable agreement with the expected mean depth of first interaction and a small bias is obtained even if the EPOS model is used to calibrate QGSJet-II events (see figure and caption for the precise values). The fitted resolutions, smaller for iron than for proton initiated showers (14.0$\pm$0.2 g cm^{-2} and 23.3$\pm$0.4 g cm^{-2}, respectively), correspond to the intrinsic fluctuations around the average $\Delta(R)$ calibration.

The experimental resolution on X_1 will, however, have other contributions which we try to estimate. The resolution of X_{max} is around 20 g cm^{-2} in the Pierre Auger Observatory [1]. The final resolution in R will depend on the accuracy with which the first part of the shower profile is reconstructed, and will be affected by the accuracy on the translation to $X' = X - X_{max}$ and the statistical error or $N' = N/N_{max}$. For typical detection in 30 g cm^{-2} and 200 observed photons at maximum (as used before in figure 3), we expect an uncertainty in R of $\pm$0.05, which leads to around 40 g cm^{-2} in Δ. So, the event-by-event resolution on X_1, in such conditions, is expected to be of the

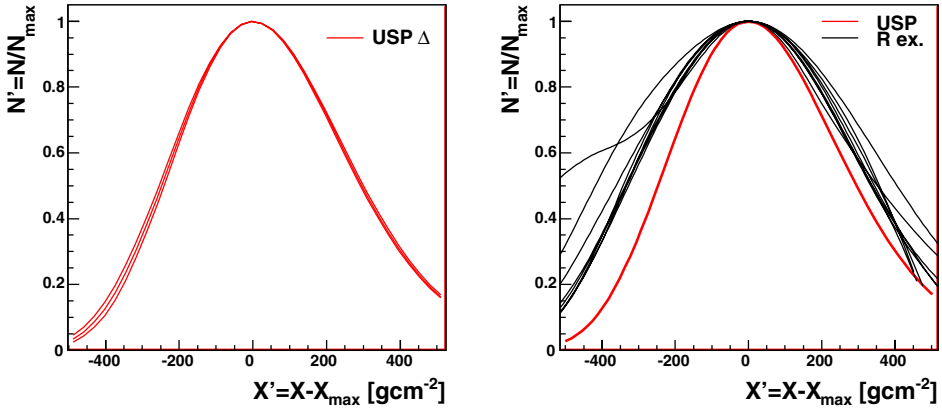

Figure 6: Average USP for showers with different $\Delta = X_{max} - X_1$ distances ($\sim$ 690; 735; 785 g cm^{-2} from bottom to top) (left). Examples of single shower profiles with R< -0.5 compared to the average USP for QGSJet-II proton showers at 10^{19}eV (right).

order of 50 g cm^{-2}.

4 Primary mass, Cross-section and Hadronic Models on a Statistical Basis

In the previous sections it was shown that R is a good primary mass composition variable with new information, and that it allows to separate the value of X_{max} into a characteristic shower length, Δ, and the depth of first interaction, X_1, leading to direct cross-section measurements. In a first approximation R is a measurement of Δ, which is different for proton and iron initiated showers. However, the relation between Δ and R is not a direct one, and even an average calibration is slightly dependent on the primary cosmic-ray particle and on the hadronic model used. In figure 5, the results obtained with the EPOS generator were shown alongside with the QGSJet-II ones. EPOS predicts larger differences between proton and iron at the level of X_{max} and R, and of Δ and X_1, but also a slightly different relation between Δ and R.

Usually, the primary mass composition analyses [1] check the evolution of the mean X_{max} and its dispersion with energy (putting together the differences of Δ and X_1, neither of them directly accessible in data), while analyses [11] of the full X_{max} distribution for each energy are used to extract a cross-section (from $1/\overline{X_1}$). The results are then compared to the predictions

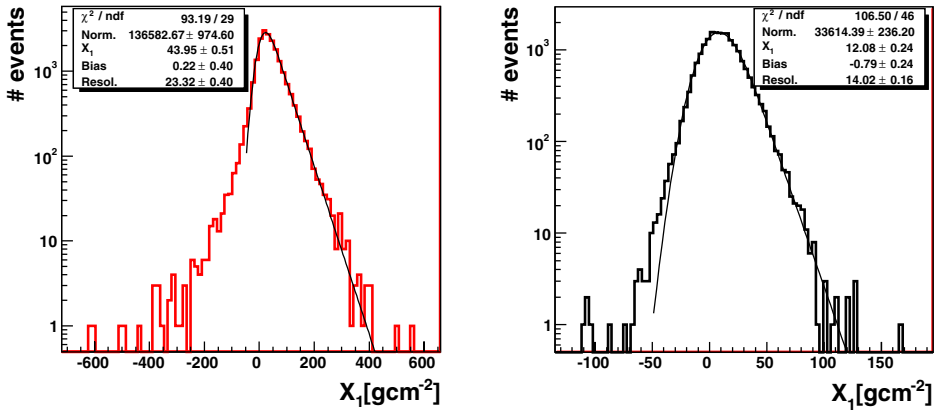

Figure 7: Reconstructed $X_1 = X_{max} + \Delta(\mathrm{R})$ distributions for proton (left) and iron(right) showers, generated with QGSJEt-II at $\log(E/eV) = 19$, with true $\overline{X_1}$=43.8 g cm^{-2} for proton and 10.6 g cm^{-2} for iron. The average calibration from fig. 5(center left) is used. If the EPOS calibration is used for the QGSJet-II events the values become: $\overline{X_1}$=44.3 ± 0.5 g cm^{-2}, Bias=0.3±0.4 g cm^{-2} and Resol.=22.6±0.4 g cm^{-2} for proton, and $\overline{X_1}$=12.5±0.2 g cm^{-2}, Bias=-1.1±0.2 g cm^{-2} and Resol.=13.0±0.4 g cm^{-2}, for iron.

of the different hadronic models for different primary particles.

Assuming that for each R value there is an almost gaussian distribution in $\bar{\Delta}$ length, it will be convoluted with an exponential in $\overline{X_1}$, to originate a given X_{max} distribution. By analysing the evolution with R of the $X_{max} = X_1 + \Delta$ distributions, at a given energy, the two pieces of information may be separated. Fig. 8 shows the parameters resulting from the fit of the convolution of an exponential in $\overline{X_1}$ and a gaussian of mean $\bar{\Delta}$ and width Σ, to the X_{max} distributions of events selected in different R bins.

The Σ of the distributions are expected to be larger for proton than for iron showers, and increase for lower R values (see fig. 5) while decreasing, by construction, for narrower R bins. The division in R thus results on a better determination of the other two fit parameters. As expected, $\bar{\Delta}$ has a strong dependence on R, while $\overline{X_1}$ is a measurement of the cross-section, independent of R in case of single primary mass composition.

In fact, the Δ(R) distributions are not exactly gaussian. Very large Δ correspond to proton showers in which the energy degradation up to the maximum was slower - in average R is smaller, but there is a larger range of R, reflecting the possibility of different shapes characteristic of the occurring phenomena. As a result, the fit can lead to a slight underestimation of $\bar{\Delta}$,

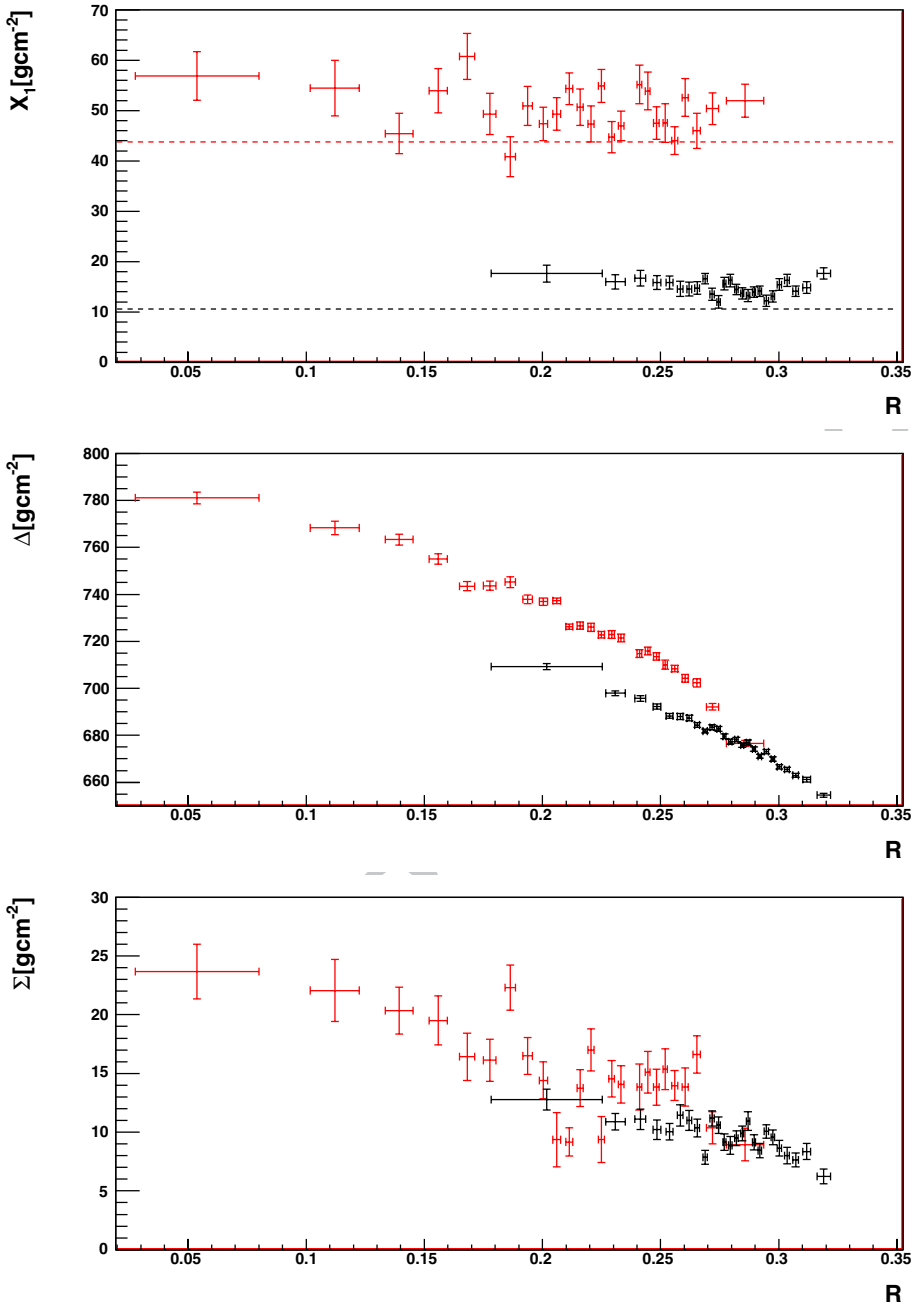

Figure 8: Fitted values of $\overline{X_1}$ (top), $\bar{\Delta}$ (center) and Σ (bottom) from the X_{max} distributions for showers selected with varying R parameter, pure proton (red) and iron (black) samples generated with QGSJet-II at $\log(E/eV) = 19$ are used. The fits were done to samples of 750 events, ordered in R (centered in the mean and with errors corresponding to the rms). The expected mean values of $\overline{X_1}$ for proton and iron are marked as horizontal lines in the top plot.

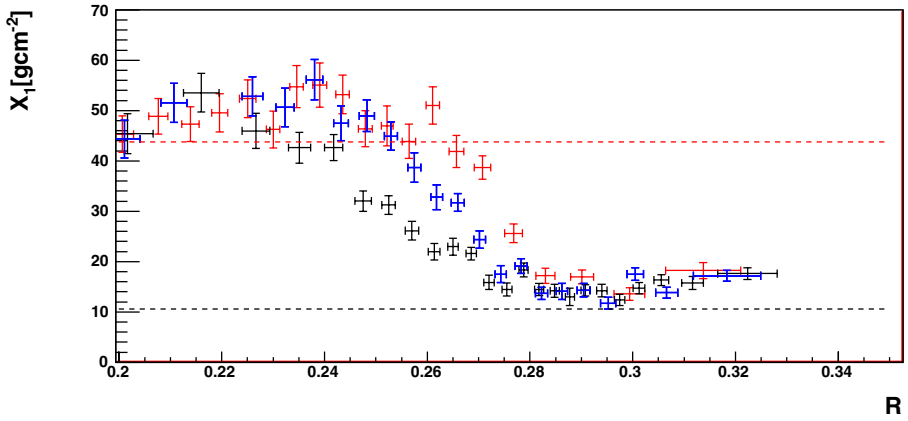

Figure 9: Fitted values of X_1 from the X_{max} distributions for showers selected with varying R parameter, pure mixed samples with 75% proton 25% iron(red), 50% proton/50% iron (blue) and 25% proton/75% iron (black) samples generated with QGSJet-II at $\log(E/eV) = 19$ are used. The fits were done to samples of 750 events, ordered in R (centered in the mean and with errors corresponding to the rms). The expected mean values of X_1 for proton and iron are marked as horizontal lines.

and corresponding overestimation of $\overline{X_1}$ in this region. For the typical Δ, however, the R value is well defined and an almost linear calibration of $\bar{\Delta}$(R) can be extracted from a fit to the data to be used in a model independent event-by-event analysis.

The results obtained for $\overline{X_1}$ for both the proton and the iron sample are in reasonable agreement with the mean first interaction depth obtained directly from the simulation, and shown by the horizontal lines. Slightly higher values of the experimental $\overline{X_1}$ are expected since (almost) elastic interactions will not contribute to initiate the electromagnetic shower and contribute to the X_{max} position.

The clear separation of the proton and iron $\overline{X_1}$ and their statistical separation in R can lead to very interesting results. Fig. 9 shows how, in case of mixed composition, stable $\overline{X_1}$ values can be found for some R ranges. Not only it represents the simultaneous measurement of the two cross-sections at the same energy, but it also helps in the definition of R cuts for the selection of almost pure composition samples for event-by-event analysis.

The above studies are done with X_{max} and R values coming from large statistics profiles and with large number of events. In the analysis of real data, the experimental resolutions of 0.05 in R and 20 g cm^{-2} in X_{max} will translate into larger uncertainties. The X_{max} resolution can be absorbed in

the allowed Σ; and the experimental resolution in R is enough to separate the extreme values of $\bar{\Delta}$ and so the $\overline{X_1}$ evolution in a limited number of bins can be obtained - with a better resolution than the 50 g cm^{-2} expected for the event-by-event analysis.

5 Conclusions

We have proposed a new parametrization of the extreme energy cosmic ray shower longitudinal profiles, based on experimentally accessible observables. In addition to the number of particles at maximum and depth of maximum, the shower is characterized by an "universal shower profile" with a characteristic, almost constant, length L (to be determined statistically from data), modified by a shape parameter R, sensitive to the primary particle type.

The shape parameter R is a measurement of the distance (Δ) between the depth of shower maximum and the depth of first interaction. The combination with X_{max} allows for the separation of the cross-section information - in the depth of first interaction - and cosmic ray composition and other hadronic model parameters - in Δ. Separate cross-section measurements and event-by-event separation of different cosmic ray primaries can be achieved.

Model independent statistical analysis can be made to check in data all the relations obtained with simulations, allowing for extra checks of different hadronic model predictions.

6 Acknowledgements

This work is partially funded by Fundação para a Ciência e Tecnologia (CERN/FP/109286/2009 and SFRH/BD/30706/2006), Portugal.

References

[1] W. Heitler, *The Quantum Theory of Radiation*, Oxford University Press, 1954.

J. Abraham [Pierre Auger Coll.]. "Measurement of the Depth of Maximum of Extensive Air Showers above 10^{18} eV". Phys. Rev. Lett. 104, 091101, 2010;

R.U. Abbasi [HiRed Coll.]. "Indications of Proton Dominated Cosmic Ray Composition above 1.6 EeV". Phy. Rev. Lett. 104, 161101, 2010;

[2] S.S. Ostapchenko. "QGSJET-II: Towards reliable description of very high energy hadronic interactions". Nucl. Phys. B (Proc. Suppl.) 151,143-146, 2006;

N.N. Kalmykov, S.S. Ostapchenko and A.I. Pavlov. and "Quark-gluon string model and EAS simulation problems at ultra-high energies". Nucl. Phys. B (Proc. Suppl.) 52,17-28, 1997.

[3] T. Pierog and K. Werner. "New facts about muon production in Extended Air Shower Simulations". Phys. Rev. Lett. 101,171101,2008;

K. Werner, F.M. Liu and T. Pierog. "Parton ladder splitting and the rapidity dependence of transverse momentum spectra in deuteron-gold collisions at RHIC". Phys. Rev. C 74,44902, 2006.

[4] T. Pierog *et al.* "First results of fast one-dimensional hybrid simulation of EAS using CONEX". Nucl.Phys.Proc.Suppl.151, 159-162, 2006. (astro-ph/0411260)

[5] M. Giller *et al.* "Energy spectra of electrons in the externsive air showers of ultra-high energy". J.Phys.G30:97,2004.

S. Lafebre *et al.* "Universality of electron-positron distributions in extensive air showers". Astropart. Phys.31:243,2009.

S. Müller, for the Pierre Auger Collaboration, "Energy Scale derived from Fluorescence Telescopes using Cherenkov Light and Shower Universality". Proc. of the 31th ICRC, 2009.

[6] M. Giller *et al.* "Similarity of extensive air showers with respect to the shower age". J.Phys.G31:947,2005.

[7] J.A.J. Matthews *et al.* "A Parametrization of Cosmic Ray Shower Profiles Based on Shower Width". J.Phys.G37:02520,2010. (arXiv:0909.4014 [astro-ph]).

[8] T.K. Gaisser and A.M. Hillas. "Reliability of the method of constant intensity cuts for reconstruction of the average development of vertical showers". Proc. of the 15th ICRC, 1977.

[9] H.M.J. Barbosa *et al.* "Determination of the calorimetric energy in extensive air showers" Astropart. Phys. 22,159-166, 2004.

[10] M. Unger *et al.* "Reconstruction of Longitudinal Profiles of Ultra-High Energy Cosmic Ray Showers from Fluorescence and Cherenkov Light Measurements" Nucl. Instrum. Meth. A588433-441, 2008.

[11] R. Ulrich *et al.* "On the measurement of the proton-air cross section using air shower data". New J. Phys. 11,065018, 2009;

K. Belov [Hires Coll.]. "p-air cross-section measurement at $10^{18.5}$ eV". Nucl.Phys.Proc.Suppl.151,197-204 , 2006.